

A SYSTEMATIC STUDY OF LOAD CARRYING CAPACITY OF ROTATIONALLY SYMMETRIC PLATES WITH THE HUBER-MISES YIELD CONDITION

J. SOKÓŁ-SUPEL and A. SAWCZUK (WARSZAWA)

Rotationally symmetric bending of rigid-plastic plates is considered, a technique of solving the plastic plate equations is developed, and a systematic presentation of design data for plates obeying the Huber-Mises yield condition is given. The proposed numerical procedure is presented first. It concerns arbitrarily loaded circular and annular plates. The collection of tables and diagrams is then given, allowing to evaluate the load carrying capacities of rotationally symmetric metal plates subjected either to pressure varying with radial coordinate or to wedge loads. The paper gives a unified presentation of the theory and design data for circular plates made of the Huber-Mises material.

1. INTRODUCTION

Limit analysis of circular and annular plates is one of the most extensively studied branches of the plastic analysis of structures. A number of solutions was obtained for particular loading and support conditions of plates with various yield criteria. An account of the theory and the solutions available can be found in the monographs [1–8].

For piece-wise linear yield criteria, both for the isotropic and anisotropic plate closed form, complete solutions to boundary value problems of incipient plastic motion of such structures are usually straightforward to obtain. In the case of nonlinear conditions of yielding, e.g., the Huber-Mises criterion for metal plates, solutions can be obtained through numerical procedures only. HOPKINS and WANG [9] produced the first results regarding the load carrying capacities of rigid-plastic circular plates under uniform pressure which obey the Huber-Mises yield criterion. EASON [10] studied velocity fields at collapse of such plates thus complementing the results obtained in Ref. [9] with explicit results. OSCHATZ [11] presented solutions for plates when taking into account the transverse shear effect on yielding. GÜNTHER and BRÄUNING [12, 13] considered anisotropic circular plates as well as plates of variable thickness and developed a suitable numerical procedure allowing also to assess the influence of anisotropy on the load carrying capacities of plates with nonlinear yield criteria.

The most extensive study of circular plates obeying the Huber-Mises yield criterion and subjected to uniformly distributed or ring loads is due to GUERLEMENT and LAMBLIN [13] who produced a set of solutions containing typical distributions

of bending moments at the yield point loads as well as the values of the load carrying capacities for several cases of boundary conditions and load arrangements.

Although the number of available solutions is quite large, there was no unified presentation of the problem both as regards the methods of numerical integration of plastic plate equations at nonlinear yield criteria as well as the load carrying capacities and the stress fields at collapse. However, for design purposes it is necessary, in addition to the principles of finding the solution, to have the results of a systematic investigation of the problem, yielding a set of tables and diagrams representing the collapse loads, bending moment fields and collapse mechanisms for various loading and boundary conditions. Such an attempt was made in [15] presenting the numerical method developed and partial results regarding complete solutions to circular and annular plate problems of limit analysis in the case of the Huber-Mises yield condition. The method was developed further to account for arbitrary rotationally symmetric loading and anisotropic nonlinear yield criteria [16].

The present paper describes a technique of integrating the equations of rotationally symmetric bending of rigid-plastic plates and gives a systematic exposition of design data for plates with the Huber-Mises yield condition. Previously available results were checked and new cases of loading were solved in order to arrive at comprehensive presentation of collapse loads and bending moments for the plates in question. The results are presented in tables and graphs thus complementing the solutions concerning the linearly elastic range [17]. Whenever elastic-plastic solutions were available, the results of the performed rigid-plastic analysis were confronted with the existing data of SOKOLOVSKI [18, 19], OHASHI and MURAKAMI [20, 21], HAYTHORTHWAITE [22] and ILIUSHIN [23].

In Section 2 the plate equations are discussed in the case of nonlinear yield criteria. The adopted numerical procedure is outlined in the next section. Section 4 contains the collapse load and bending moments for circular plates under various types of distributed loads. The results regarding partially loaded circular plates as well as statically determinate annular plates are given in Sections 5 and 6. Section 7 deals with annular plates supported or clamped on both boundaries. The final section contains some concluding remarks. The collection of tables and diagrams allows to assess the load carrying capacities of rotationally symmetric metal plates in typical situations occurring in technology.

2. PLATE EQUATIONS

In rotationally symmetric loading and boundary conditions plastic bending of circular and annular plates is governed by ordinary differential equations. The net of principal lines of moments and curvatures defines a system of polar coordinates on the plate middle surface. A plate element and the coordinate system R, θ are shown in Fig. 1 where the adopted notation and the sign convention for the stress resultants as well as for the displacement velocity are also specified.

Let B denote the outer radius and M_0 be the plate yield moment. The rates of curvature of the deflected surface W are denoted by K_r and K_θ , whereas the radial and the circumferential bending moments are M_r and M_θ , respectively, and S_r ,

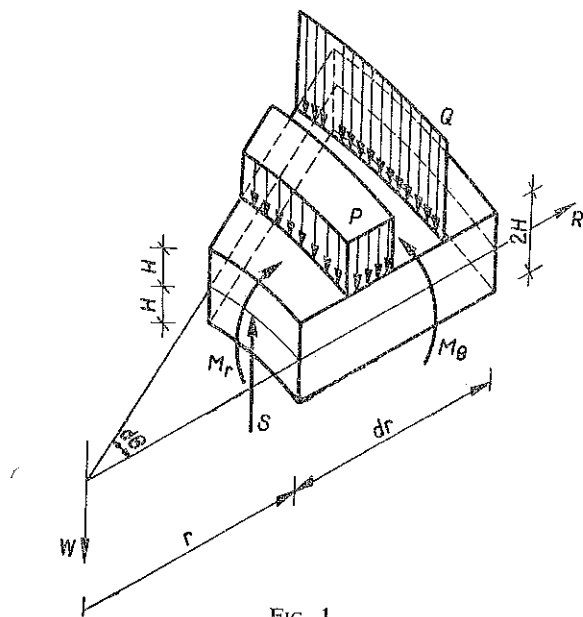


FIG. 1.

denotes the radial transverse shear. The following dimensionless quantities will be employed in the analysis:

$$(2.1) \quad r = \frac{R}{B}, \quad w = \frac{WH}{B^2}, \quad \kappa_r = HK_r, \quad \kappa_\theta = HK_\theta,$$

$$m_r = \frac{M_r}{M_0}, \quad m_\theta = \frac{M_\theta}{M_0}, \quad s = \frac{S_r B}{M_0}.$$

The dimensionless distributed pressure and line load are, respectively,

$$(2.2) \quad \mu p = \frac{PB^2}{M_0}, \quad \mu q = \frac{QB}{M_0},$$

where μ denotes the collapse load multiplier.

The complete solution of a limit analysis problem for a plate consists in finding the collapse load corresponding to the incipient plastic motion, the bending moment distribution associated with the collapse load, and a deflection velocity of the plate middle surface.

The set of equations consists of the equilibrium requirements

$$(2.3) \quad (rs)' + rp\mu = 0, \quad (rm_r)' - m_\theta - rs = 0$$

the curvature—displacement relations

$$(2.4) \quad \kappa_r = -w'', \quad \kappa_\theta = -\frac{w'}{r},$$

a yield condition

$$(2.5) \quad F(m_r, m_\theta) - 1 = 0 \quad \text{or} \quad m_\theta = f(m_r)$$

and the plastic potential flow law

$$(2.6) \quad (\kappa_r, \kappa_\theta) = v \left(\frac{\partial F}{\partial m_r}, \frac{\partial F}{\partial m_\theta} \right), \quad v \geq 0$$

with an appropriate generalization in the case of yield loci with singularities.

The plate equations split into two systems. Equations (2.3) and (2.5) reduce to the following single equation:

$$(2.7) \quad (rm_r)' - f(m_r) + \mu \int \rho p \, d\rho + C = 0$$

and the bending moment field can be specified if stress boundary conditions are prescribed.

The deflection velocity is governed by the equation

$$(2.8) \quad rw'' + w' \frac{dm_\theta}{dm_r} = 0,$$

which follows from Eqs. (2.4) and (2.5). The deflection rate field depends on the slope of the yield curve (2.5) and contains hinge lines. A circular hinge forms when

$$(2.9) \quad \frac{\kappa_r}{\kappa_\theta} = r \frac{w''}{w'} \rightarrow \infty$$

and the slope of the deflected surface W suffers then a discontinuity, $[w'] \neq 0$. Such a circumferential hinge corresponds to these points of the yield curve (2.5) where

$$(2.10) \quad \frac{dm_r}{dm_\theta} = 0.$$

The usual procedure of solving plate equations consists in integrating Eq. (2.7) and then finding the associated velocity field from Eq. (2.8) for the boundary conditions in question.

The boundary conditions are at the free edge

$$(2.11) \quad w = w_0, \quad m_r = 0,$$

at the simply supported boundary

$$(2.12) \quad w = 0, \quad m_r = 0$$

and at the clamped edge of the plate

$$(2.13) \quad w = 0 \text{ and } w' = 0 \text{ or } [w'] \neq 0 \rightarrow m_r = \text{extr } m_r,$$

according to Eq. (2.10).

For a nonlinear yield condition the resulting differential equations are nonlinear and require numerical procedures to arrive at the solution. At this stage there are no differences between isotropic and orthotropic plates provided the principal direction of moments and curvatures coincide with those of orthotropy.

Once the bending moments and the deflection velocity are obtained from Eqs. (2.7) and (2.8), there still remains to check the non-negativeness of the flow multiplier v appearing in the associated flow law (2.6), thus

$$(2.14) \quad v = -\frac{w'}{r} / \frac{\partial F}{\partial m_\theta} > 0$$

in plastically deforming regions.

3. NUMERICAL PROCEDURE

We shall consider plates with the Huber-Mises yield condition

$$(3.1) \quad F = m_r^2 - m_r m_\theta + m_\theta^2 - 1 = 0,$$

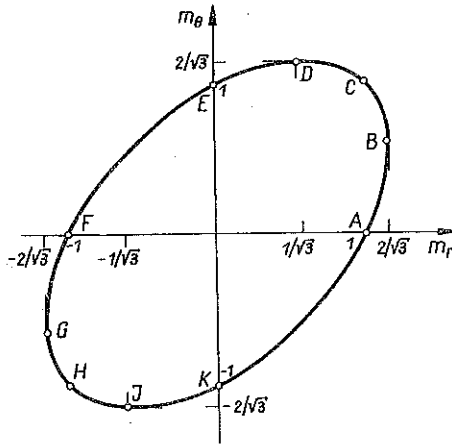


FIG. 2.

shown in Fig. 2. Circumferential hinge lines, according to Eq. (2.10), appear for the stress states B and G marked on the yield ellipse in Fig. 2 and corresponding to

$$(3.2) \quad m_r = 2m_\theta = \pm \frac{2}{\sqrt{3}}.$$

Equation (2.7) specifying the radial moment becomes

$$(3.3) \quad \frac{dm_r}{dr} = \frac{1}{r} \left(-\frac{1}{2} m_r \pm \frac{1}{2} \sqrt{4 - 3m_r^2 + sr} \right),$$

where

$$(3.4) \quad sr = -\mu \left\{ \sum_1^{k-1} \int_{c_j}^{c_{j+1}} p_j \rho \, d\rho + \int_{c_k}^r p_k \rho \, d\rho + \sum_1^l q_i b_i - \beta \frac{T}{2\pi} \right\}$$

and μT denotes the total load acting on the plate, hence

$$(3.5) \quad T = 2\pi \left\{ \sum_1^m \int p_j \rho \, d\rho + \sum_1^n q_i b_i \right\}.$$

In Eq. (3.4) β denotes the reaction at an internal support. The notation employed is defined in Fig. 3 representing a radial section of an annular plate under stepwise loading.

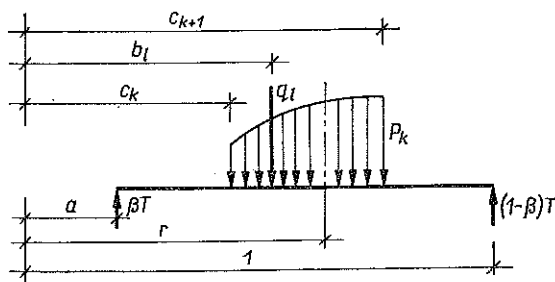


FIG. 3.

For statically determinate cases, $\beta=0$ or $\beta=1$, Eq. (3.3) can be integrated for the appropriate stress boundary conditions. Otherwise, the integration of Eq. (3.3) is accompanied by solving the equation governing the displacement velocity.

For the Huber-Mises yield condition Eq. (2.8) takes the form

$$(3.6) \quad 2rw'' + w' \left(1 \mp \frac{3m_r}{\sqrt{4-3m_r^2}} \right) = 0,$$

since

$$(3.7) \quad m_\theta = \frac{1}{2} (m_r \pm \sqrt{4-3m_r^2}).$$

Its solution is

$$(3.8) \quad w = C_1 \int_a^r \exp \left[\int_a^\rho \frac{1}{2t} \left(\pm \frac{3m_r}{\sqrt{4-3m_r^2}} - 1 \right) dt \right] d\rho + C_2,$$

whereas C_1 and C_2 are to be determined from the kinematical boundary conditions.

For statically indeterminate cases a missing condition for evaluating the reaction β entering Eq. (3.4) is that of changing the sign of the circumferential curvature of the deflection velocity (3.8). Requiring

$$(3.9) \quad K_\theta = 0 \quad \text{thus} \quad w' = 0$$

one obtains $r=r^*$ such that $w(r^*)=w_0$ and

$$(3.10) \quad m_r(r^*) = \pm \frac{2}{\sqrt{3}}, \quad \left. \frac{dm_r}{dr} \right|_{r=r^*} = 0$$

hence r^* is obtained from the equation

$$(3.11) \quad sr \mp \frac{1}{\sqrt{3}} = 0,$$

which specifies the radius where the stress profile changes from the upper part of the yield ellipse in Fig. 2 to the lower part *BAKJHG*.

A computer program was developed to yield numerical solutions to Eqs. (3.3) and (3.8). The flow chart and details of the program concerning the Huber-Mises yield condition can be found on [15] and for an arbitrary nonlinear yield condition in [16]. The essentials of the adopted procedure will only be given here in order to make the numerical values presented in the following sections easy to interpret.

The program was arranged in three routines regarding the stress profile on the yield condition. The first group of problems concerned the equation

$$(3.12) \quad \frac{dm_r}{dr} = \frac{1}{r} \left(-\frac{1}{2} m_r + \frac{1}{2} \sqrt{4 - 3m_r^2 + sr} \right),$$

where

$$(3.13) \quad sr = -\mu \left\{ \sum_1^{k-1} \int_{c_j}^{c_{j+1}} p_j \rho \, d\rho + \int_{c_k}^r p_k \rho \, d\rho + \sum_1^l q_i b_i \right\}$$

under the conditions, respectively,

$$(3.14) \quad m_r(a) = \begin{cases} 1, \\ \frac{2}{\sqrt{3}} \\ 0 \end{cases} \quad \text{and} \quad m_r(1) = 0 \quad , \text{ or} \quad m_r(1) = \frac{-2}{\sqrt{3}}.$$

The kinematical conditons for Eq. (3.8) were

$$(3.15) \quad w(a) = w_0, \quad w(1) = 0.$$

This group of problems therefore contained circular plates, plates with a rigid central boss as well as annular plates with the internal edge free. The stress profile thus belonged to the part *BCDEFG* of the yield ellipse in Fig. 2. Equation (3.12) was integrated using the Runge-Kutta fourth-order method so as to meet the prescribed-value at the outer boundary and thus find the corresponding value of the collapse load multiplier μ .

The second group of problems considered was goverened by the equation

$$(3.16) \quad \frac{dm_r}{dr} = \frac{1}{r} \left(-\frac{1}{2} m_r - \frac{1}{2} \sqrt{4 - 3m_r^2 + sr} \right)$$

and Eq. (3.4) with $\beta=1$, under the conditions

$$(3.17) \quad m_r(1)=0 \quad \text{and} \quad m_r(a)=0 \quad \text{or} \quad m_r(a)=-\frac{2}{\sqrt{3}}.$$

The kinematical boundary conditions for Eq. (3.8) were

$$(3.18) \quad w(a)=0, \quad w(1)=w_0.$$

This group consisted thus of annular plates with the outer edge free. The stress profile belonged to the part *BAKIHG* of the yield locus in Fig. 2. The integration technique was the same as in the previous case.

The last group of studied problems concerned statically indeterminate plates, thus annular plates hinged or clamped at both circumferences. For $a \leq r \leq r^*$ Eq. (3.16), is applied, whereas in the range $r^* \leq r \leq 1$ Eq. (3.12) should be applied, under the conditions

$$(3.19) \quad m_r(a)=\begin{cases} 0 \\ -\frac{2}{\sqrt{3}} \end{cases} \quad \text{and} \quad m_r(1)=0 \quad \text{or} \quad m_r(1)=-\frac{2}{\sqrt{3}}.$$

Moreover,

$$(3.20) \quad m_r(r^*)=\frac{2}{\sqrt{3}}$$

according to the requirement (3.9), whereas r^* is obtained from Eq. (3.11). Equations (3.12) and (3.16) are solved using Eq. (3.4). The computation procedure is now more involved since the reaction β has to be determined using the information available from the transverse velocity field (3.8), and specifically the requirements (3.9). The kinematical boundary conditions are

$$(3.21) \quad w(a)=0, \quad w(r^*)=w_0, \quad w(1)=0.$$

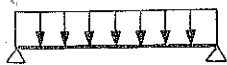
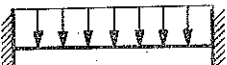




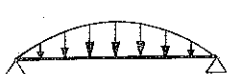
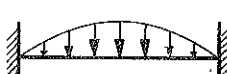


The solution procedure requires several trials involving resolutions of Eq. (3.11), and the technique is explained in [15].

The program allows to find the complete limit analysis solutions for rotationally symmetric plates subjected to an arbitrary number of wedge loads and piece-wise continuous distributed loads as indicated in Fig. 3. The entire plate is in a plastic state and the bending moments are continuous. The program computes values of the collapse load multiplier with a prescribed accuracy ε . The results given in the tables have the accuracy $\varepsilon(\mu)=0.001$. The program prints the collapse load multiplier μ , the reaction β , the radius r^* of the stress profile change as well as the values m_r , m_θ and w at the required points of the plate radius.

4. CIRCULAR PLATES UNDER DISTRIBUTED LOADS

For simply supported circular plates subjected to downwards directed distributed loading the stress profile corresponds to the segment *CDE* of the yield ellipse of Fig. 2. When the plate circumference is clamped, the stress profile extends over the region *CDEFG*.

Table 1

Simply supported	Load carrying capacity		Clamped	Lad carrying capacity	
	μ	Total load		μ	Total load
	6.517	20.472		12.551	39.431
	13.074	13.691		24.316	25.463
	12.848	26.907		25.454	53.309
	9.322	14.643		17.515	27.511
	21.189	33.283		42.687	67.053

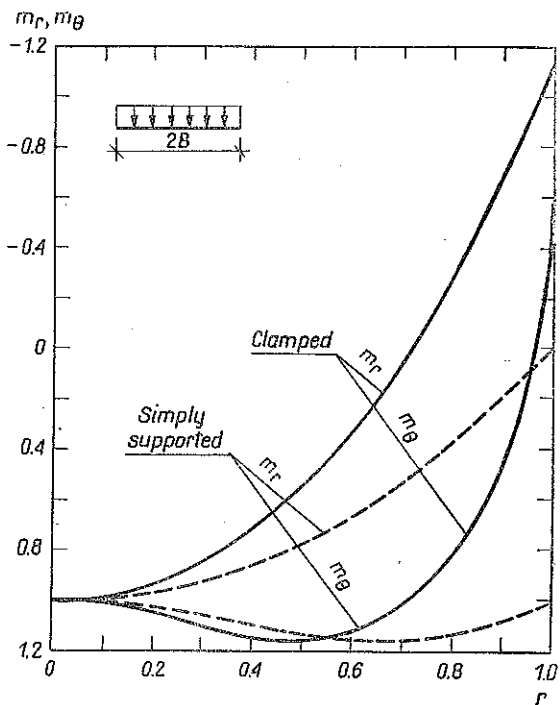


FIG. 4.

Table 2

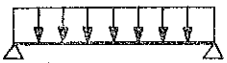
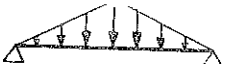



Loading	Bending moments and								
	r	0.000	0.050	0.100	0.150	0.20	0.25	0.30	0.35
 $\mu = 6.517$	m_r	1.000	0.998	0.992	0.981	0.967	0.947	0.924	0.896
	m_θ	1.000	1.002	1.008	1.017	1.030	1.045	1.061	1.078
	w/w_0	1.000	0.991	0.978	0.955	0.924	0.886	0.841	0.792
 $\mu = 13.074$	m_r	1.000	0.995	0.984	0.966	0.940	0.908	0.869	0.825
	m_θ	1.000	1.004	1.015	1.031	1.051	1.072	1.093	1.112
	w/w_0	1.000	0.989	0.972	0.945	0.909	0.865	0.816	0.762
 $\mu = 12.848$	m_r	1.000	1.000	0.999	0.998	0.993	0.987	0.977	0.963
	m_θ	1.000	1.000	1.001	1.003	1.007	1.013	1.022	1.034
	w/w_0	1.000	0.993	0.983	0.965	0.940	0.909	0.870	0.826
 $\mu = 9.322$	m_r	1.000	0.997	0.988	0.974	0.953	0.926	0.894	0.855
	m_θ	1.000	1.003	1.011	1.025	1.041	1.060	1.080	1.100
	w/w_0	1.000	0.990	0.975	0.949	0.915	0.873	0.826	0.773
 $\mu = 21.189$	m_r	1.000	1.000	1.000	0.999	0.999	0.997	0.993	0.987
	m_θ	1.000	1.000	1.000	1.001	1.001	1.003	1.008	1.013
	w/w_0	1.000	0.994	0.985	0.969	0.947	0.919	0.884	0.844

Table 3






Loading	Bending moments and								
	r	0.000	0.050	0.100	0.150	0.20	0.25	0.30	0.35
 $\mu = 12.551$	m_r	1.000	0.996	0.984	0.964	0.935	0.898	0.850	0.793
	m_θ	1.000	1.004	1.015	1.033	1.054	1.078	1.102	1.123
	w/w_0	1.000	0.988	0.970	0.939	0.899	0.852	0.798	0.740
 $\mu = 24.316$	m_r	1.000	0.992	0.971	0.935	0.886	0.824	0.749	0.661
	m_θ	1.000	1.008	1.027	1.054	1.084	1.113	1.136	1.150
	w/w_0	1.000	0.984	0.960	0.923	0.874	0.819	0.758	0.696
 $\mu = 25.054$	m_r	1.000	1.000	0.998	0.994	0.986	0.973	0.953	0.925
	m_θ	1.000	1.000	1.002	1.006	1.013	1.025	1.041	1.061
	w/w_0	1.000	0.992	0.979	0.958	0.928	0.890	0.846	0.795
 $\mu = 17.515$	m_r	1.000	0.994	0.978	0.950	0.910	0.858	0.794	0.717
	m_θ	1.000	1.006	1.021	1.044	1.071	1.098	1.123	1.142
	w/w_0	1.000	0.986	0.964	0.930	0.885	0.832	0.774	0.712
 $\mu = 42.687$	m_r	1.000	1.000	1.000	0.999	0.997	0.993	0.986	0.973
	m_θ	1.000	1.000	1.000	1.001	1.003	1.007	1.014	1.025
	w/w_0	1.000	0.993	0.983	0.965	0.940	0.908	0.869	0.823

Table 2 [cont.]

deflection velocities												
0.40	0.45	0.50	0.55	0.60	0.65	0.70	0.75	0.80	0.85	0.90	0.95	1.00
0.862	0.823	0.779	0.730	0.675	0.613	0.546	0.472	0.392	0.304	0.210	0.115	0.000
1.096	1.112	1.127	1.139	1.148	1.153	1.154	1.148	1.136	1.116	1.088	1.052	1.000
0.738	0.681	0.621	0.559	0.497	0.433	0.370	0.306	0.243	0.181	0.119	0.059	0.000
0.776	0.722	0.663	0.602	0.537	0.469	0.401	0.331	0.261	0.193	0.126	0.061	0.000
1.129	1.141	1.150	1.154	1.154	1.148	1.138	1.124	1.105	1.082	1.057	1.029	1.000
0.705	0.646	0.586	0.525	0.464	0.403	0.342	0.282	0.224	0.166	0.109	0.054	0.000
0.944	0.920	0.889	0.851	0.805	0.749	0.683	0.605	0.515	0.410	0.219	0.154	0.000
1.048	1.064	1.083	1.101	1.120	1.136	1.148	1.154	1.153	1.140	1.113	1.068	1.000
0.777	0.722	0.664	0.602	0.537	0.471	0.404	0.335	0.267	0.199	0.132	0.065	0.000
0.810	0.760	0.705	0.645	0.580	0.511	0.440	0.366	0.291	0.216	0.141	0.069	0.000
1.118	1.133	1.145	1.152	1.155	1.152	1.145	1.131	1.113	1.090	1.063	1.033	1.000
0.717	0.658	0.598	0.537	0.475	0.413	0.351	0.290	0.230	0.170	0.112	0.056	0.000
0.977	0.963	0.944	0.917	0.882	0.836	0.776	0.704	0.612	0.499	0.362	0.197	0.000
1.021	1.033	1.048	1.066	1.086	1.108	1.128	1.145	1.154	1.151	1.131	1.084	1.000
0.798	0.745	0.689	0.628	0.564	0.497	0.427	0.356	0.284	0.212	0.141	0.070	0.000

Table 3 [cont.]

deflection velocities												
0.40	0.45	0.50	0.55	0.60	0.65	0.70	0.75	0.80	0.85	0.90	0.95	1.00
0.725	0.646	0.555	0.452	0.336	0.206	0.063	-0.095	-0.269	-0.459	-0.668	-0.898	-1.155
1.141	1.152	1.154	1.146	1.125	1.087	1.030	0.949	0.838	0.688	0.482	0.180	-0.576
0.679	0.616	0.553	0.490	0.428	0.367	0.307	0.250	0.194	0.141	0.091	0.044	0.000
0.562	0.453	0.334	0.206	0.071	-0.071	-0.218	-0.369	-0.522	-0.678	-0.835	-0.993	-1.155
1.155	1.146	1.124	1.087	1.036	0.963	0.873	0.764	0.631	0.471	0.274	0.015	-0.576
0.632	0.568	0.505	0.443	0.383	0.326	0.271	0.218	0.168	0.121	0.077	0.037	0.000
0.887	0.838	0.775	0.696	0.599	0.482	0.342	0.177	-0.016	-0.241	-0.501	-0.803	-1.155
1.084	1.107	1.129	1.146	1.154	1.150	1.126	1.077	0.992	0.857	0.650	0.317	-0.576
0.739	0.678	0.616	0.551	0.485	0.419	0.354	0.289	0.227	0.166	0.107	0.052	0.000
0.628	0.526	0.413	0.289	0.154	0.011	-0.141	-0.300	-0.464	-0.632	-0.803	-0.977	-1.155
1.153	1.153	1.140	1.113	1.068	1.005	0.922	0.816	0.684	0.521	0.317	0.045	-0.576
0.650	0.585	0.522	0.459	0.399	0.339	0.283	0.228	0.177	0.127	0.081	0.039	0.000
0.954	0.926	0.885	0.831	0.757	0.661	0.538	0.381	0.186	-0.057	-0.352	-0.714	-1.155
1.041	1.061	1.085	1.110	1.134	1.150	1.154	1.135	1.080	0.971	0.776	0.429	-0.576
0.772	0.715	0.654	0.590	0.523	0.455	0.386	0.317	0.250	0.183	0.119	0.058	0.000

The load carrying capacities for several cases of loading are given in Table 1. The values originally obtained in Ref. [12] are thus either reconfirmed or improved.

In Table 2 the bending moments at the plate collapse as well as the deflection velocities at the incipient plastic motion are given for simply supported plates at various loading conditions. Table 3 contains analogous results for clamped plates.

In order to visualize the differences in the bending moment distributions for simply supported and clamped plates, Fig. 4 given the respective diagrams concerning uniformly distributed loads. For other loading conditions appropriate diagrams can be found in [15]. A comparison of the respective deflection velocities is given in Fig. 5. The characteristic inflection point of the velocity profile corresponds

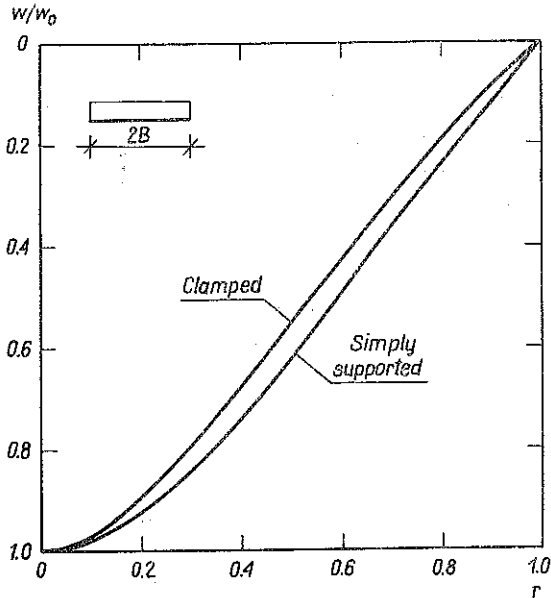


FIG. 5.

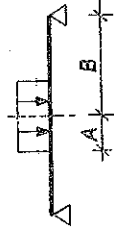
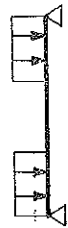
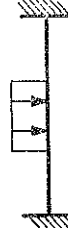



to the stress state represented by the point *D* on the yield curve of Fig. 2. For the other distributed loading the displacement velocities have similar profiles except that the inflection point occurs at slightly different radii. This can easily be seen in Tables 2 and 3.

5. PARTIALLY-LOADED CIRCULAR PLATES

The load carrying capacities for plates loaded over an annulus or over a circle are given in Table 4. In all these cases the stress profile runs over the part *CDEFG* of the yield locus in Fig. 2.

Typical distributions of bending moments for plates loaded over a central area are shown in Figs. 6 and 7 for simply supported and clamped plates, respectively. It is to be remarked that when the loaded area shrinks, the bending moment for

Table 4

Loading		Collapse load										
		α	0.000	0.10	0.20	0.30	0.40	0.50	0.60	0.70	0.80	0.90
	μ	—	226.500	61.687	29.375	18.375	12.969	10.016	8.281	7.258	6.703	6.517
	T	2π	7.115	7.751	8.446	9.236	10.185	11.327	12.747	14.592	17.056	20.473
	μ	6.517	6.680	7.188	8.1586	9.766	12.547	17.656	28.531	58.750	216.189	—
	T	20.473	20.775	21.678	23.316	25.771	29.562	35.498	45.711	66.442	129.044	—
	μ	—	349.437	100.594	50.625	32.141	23.266	18.367	15.484	13.766	12.844	12.551
	T	$\frac{4\pi}{\sqrt{3}}$	10.997	12.640	14.313	16.155	18.272	20.772	23.835	27.677	32.683	39.429
	μ	12.551	12.898	14.004	16.031	19.453	25.312	36.094	59.094	123.250	459.606	—
	T	39.429	40.113	42.233	45.829	51.334	59.698	72.569	94.678	138.388	274.340	—
	μ	—	11.766	6.648	5.055	4.398	4.195	4.336	4.906	6.375	11.219	—
	T	2π	7.392	8.354	9.528	11.053	13.178	16.346	21.577	32.043	63.440	—
	μ	—	18.676	11.262	8.971	8.109	7.984	8.492	9.875	13.152	23.680	—
	T	$\frac{4\pi}{\sqrt{3}}$	11.734	14.152	16.909	20.375	25.082	37.031	43.431	66.107	133.903	—

a simply supported plate tends to a singular distribution disclosed in [9, 10] for point-loaded plates. For clamped plates discontinuities are expected both at the center and at the support in the case of a point loaded plate [9].

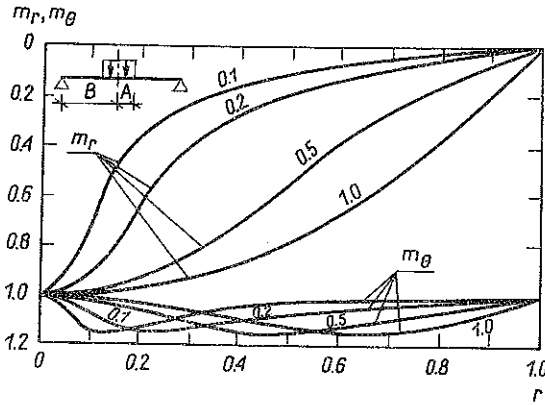


FIG. 6.

For plates loaded by ring of forces, characteristic bending moment distributions are shown in Fig. 8 and 9. Since the stress profiles are similar to the previous cases, the bending moments have a similar form, except that in the zone $0 \leq r \leq a$ homogeneous bending takes place, the stress profile being represented by the point C of the yield locus of Fig. 2.

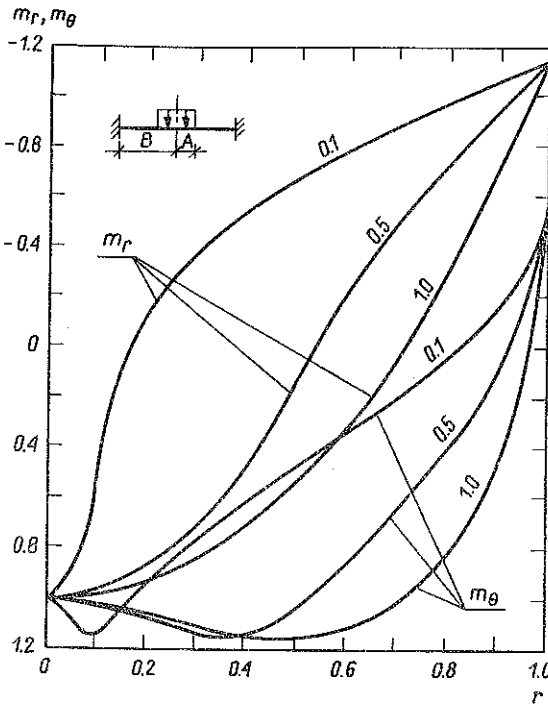


FIG. 7.

Figure 10 shows the deflection velocities for centrally-loaded plates. Quite similar shapes are obtained for a ring loading, except that the zone $0 \leq r \leq a$ then deforms into a sphere since both the curvatures are equal for the stress point C of the yield

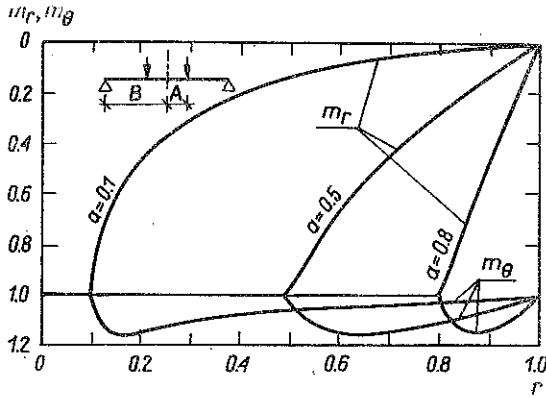


FIG. 8.

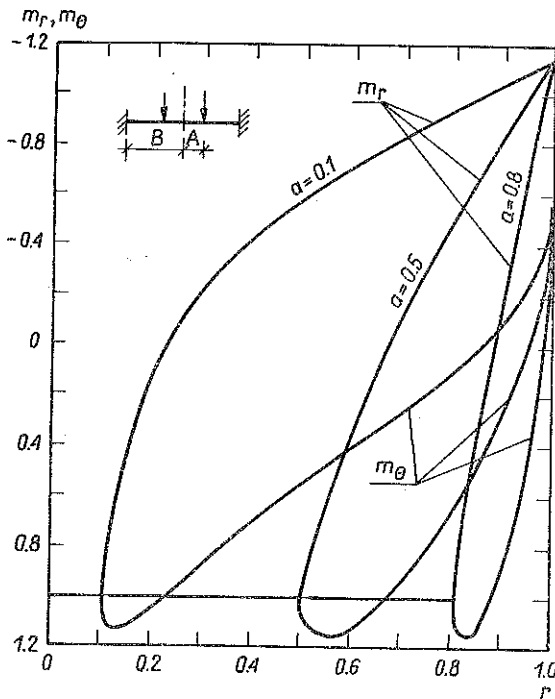


FIG. 9.

locus. With a broken line in Fig. 10, the appropriate velocity field is shown for a plate loaded at the center by a concentrated force and simply supported. The velocity field is then $w = w_0 (1 - \sqrt{r})$, [10].

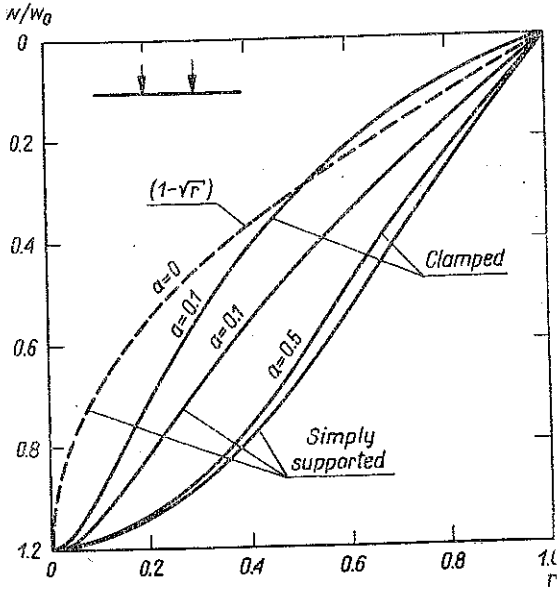


FIG. 10.

6. ANNULAR PLATES

For annular plates governed by Eq. (3.19) the load carrying capacities are assembled in Table 5. Typical diagrams of bending moments are given in Figs. 11 and 12. In the case of a simply supported plate with the central opening, characteristic features of the radial moment distribution have to be pointed out. The stress profiles

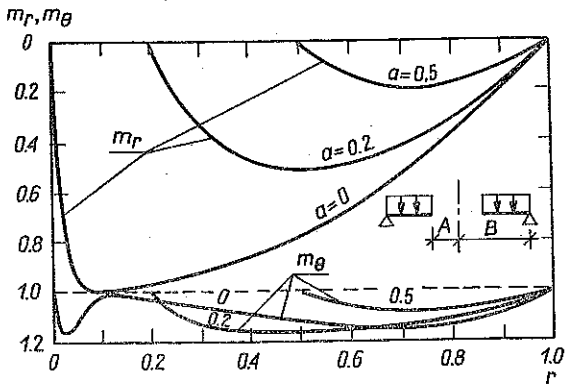
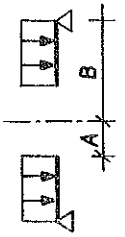

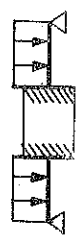
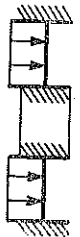
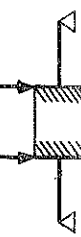



FIG. 11.

run then over the segment EDB so that all the points of the respective part of the yield curve are attained twice. The corresponding bending moments are plotted in Fig. 11.

Table 5

Loading	Collapse load												
	a	0.00	0.10	0.20	0.30	0.40	0.50	0.60	0.70	0.80	0.90	0.95	
	μ	6.515	6.270	5.984	5.875	5.984	6.359	7.109	8.594	11.750	21.625	41.557	
	T	20.468	17.924	18.046	16.795	16.167	14.982	14.293	13.769	13.288	13.907	13.907	12.729
	μ	12.550	12.352	12.504	13.355	15.164	18.492	24.781	38.125	74.813	262.250	984.058	
	T	39.426	38.416	37.910	38.178	40.015	43.569	49.824	61.082	84.609	156.533	301.422	
	μ	6.516	6.700	7.270	8.326	10.112	13.178	18.853	30.979	65.005	244.231	949.211	
	T	20.470	20.838	21.926	23.802	26.685	31.049	37.906	49.566	73.518	145.782	290.748	
	μ	12.551	12.933	14.106	16.257	19.870	26.044	37.437	61.764	129.893	488.600	1899.054	
	T	39.429	40.224	42.542	46.476	52.435	1.364	75.271	98.959	146.905	291.648	581.690	
	μ	—	11.931	6.828	5.256	4.634	4.478	4.692	5.394	7.123	12.743	24.225	
	T	—	7.496	8.580	9.907	11.646	14.068	17.688	23.724	35.804	72.060	144.599	
	μ	—	18.961	11.517	9.232	8.395	8.315	8.893	10.399	13.929	25.221	48.220	
	T	—	11.913	14.472	17.402	21.098	26.122	33.523	45.737	70.014	142.621	287.827	

If a plate is furnished with a rigid boss covering the central area, the stress profile contains the point *B* of the yield locus of Fig. 2 and runs up to the point *E* or *G*, depending upon the boundary conditions at the outer circumference. A characteristic set of bending moment diagrams is shown in Fig. 12. The distribution of moments, at the boss is to be pointed out. Further examples of moment fields can be found in [15]. No essentially new features, however, are noticed.

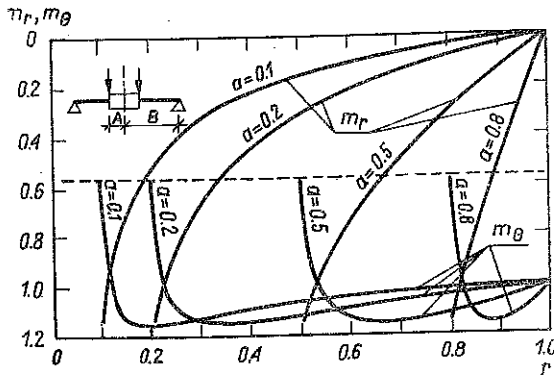


FIG. 12.

Annular plates, supported or clamped at the inner circumference, are governed by Eq. (3.16) and therefore the corresponding stress profiles run over the part *BAKIHG* of the yield curve in Fig. 2. The load carrying capacities are given in Table 6, whereas Figs. 13 and 14 give bending moments. Some of the results presented

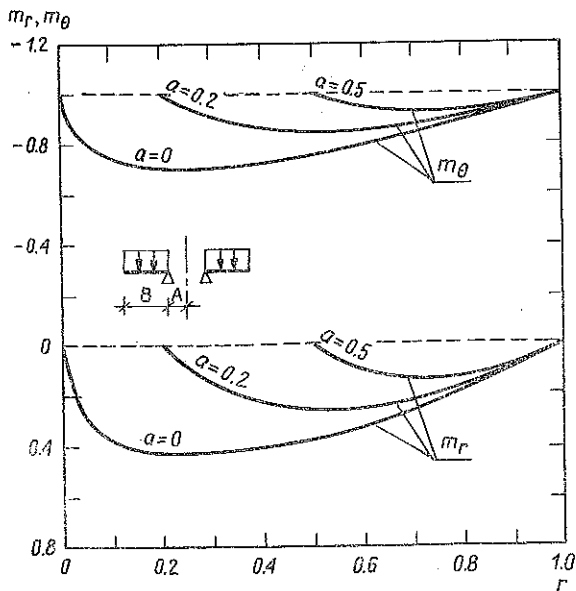


FIG. 13.

were obtained earlier by GUERLEMENT and LAMBLIN [14]. It is interesting to note the bending moment field at $a \rightarrow 0$ depending on whether the plate is simply supported or clamped.

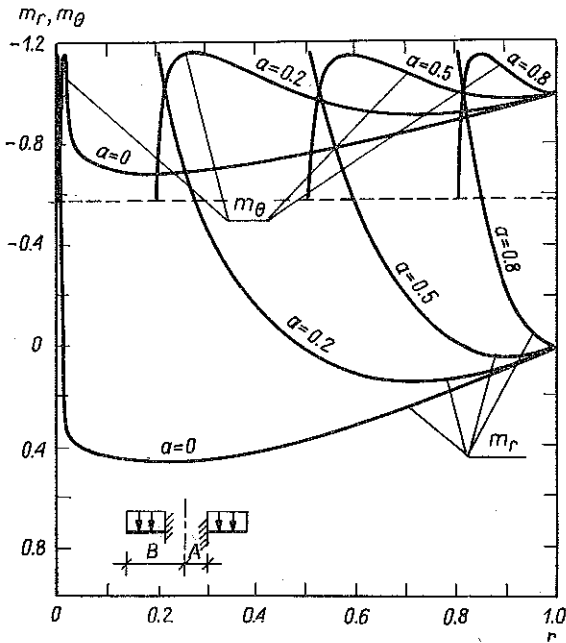


FIG. 14.

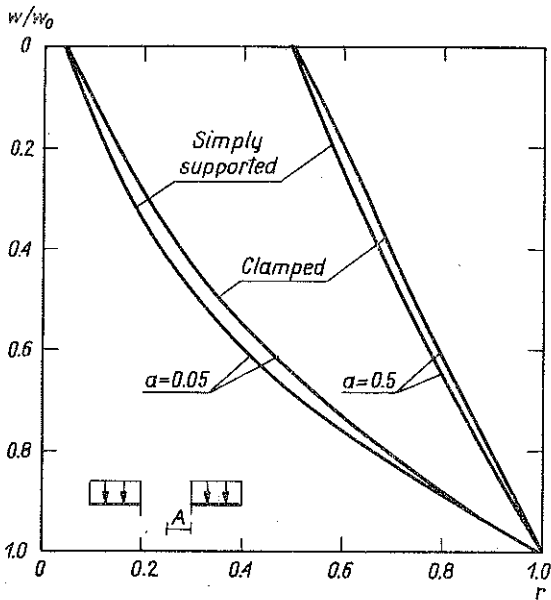


FIG. 15.

The deflection velocity profile is shown in Fig. 15 for the considered cantilever annular plates.

Table 6

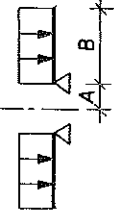
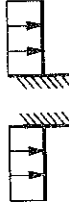


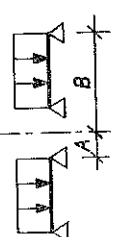
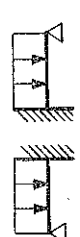
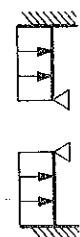
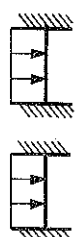
Loading and support conditions	Collapse load												
	a	0.05	0.1	0.2	0.3	0.4	0.5	0.6	0.7	0.8	0.9	0.95	
	μ	2.620	2.763	3.061	3.417	3.891	4.555	5.531	7.211	10.547	20.625	40.503	
	T	8.209	8.593	9.232	9.769	10.268	10.732	11.121	11.554	11.928	12.311	12.406	
	μ	3.025	3.437	4.359	5.619	7.484	10.531	16.039	27.758	60.859	236.875	935.722	
	T	9.481	10.690	13.146	16.064	19.750	24.813	32.248	44.474	68.830	141.339	286.616	
	μ	1	1	1	1	1	1	1	1	1	1	1	
	T	2π	2π	2π	2π	2π	2π	2π	2π	2π	2π	2π	
	μ	1.112	1.193	1.366	1.577	1.854	2.238	2.815	3.776	5.698	11.469	23.015	
	T	6.986	7.496	8.580	9.907	11.647	14.065	17.689	23.725	35.802	72.062	144.606	

Table 7

Loading and support conditions		Load carrying capacity									
		a	0.05	0.1	0.2	0.3	0.4	0.5	0.6	0.7	0.8
	μ	13.812	15.252	18.692	25.531	30.881	42.833	64.767	111.651	243.712	946.630
	T	43.283	47.436	56.692	67.272	81.493	100.923	130.222	178.889	275.632	565.046
	β	0.268	0.293	0.333	0.366	0.393	0.418	0.438	0.456	0.473	0.487
	μ	15.263	17.434	22.424	29.280	39.653	56.581	87.543	153.961	343.071	1359.593
	T	47.829	54.223	67.629	83.707	104.642	133.316	176.016	246.678	388.004	811.545
	β	0.298	0.333	0.368	0.427	0.460	0.489	0.513	0.535	0.554	0.571
	μ	21.174	23.184	28.023	34.999	45.635	63.229	95.040	163.617	356.662	1382.386
	T	66.353	72.106	84.515	100.057	120.428	148.980	191.089	262.149	403.375	825.150
	β	0.182	0.206	0.245	0.277	0.304	0.328	0.350	0.368	0.385	0.401
	μ	22.947	25.900	32.709	42.174	56.381	79.916	122.846	214.653	475.674	1873.782
	T	71.910	80.554	98.648	120.569	148.786	188.298	246.997	343.920	537.975	1118.465
	β	0.219	0.242	0.293	0.334	0.368	0.397	0.423	0.446	0.466	0.484

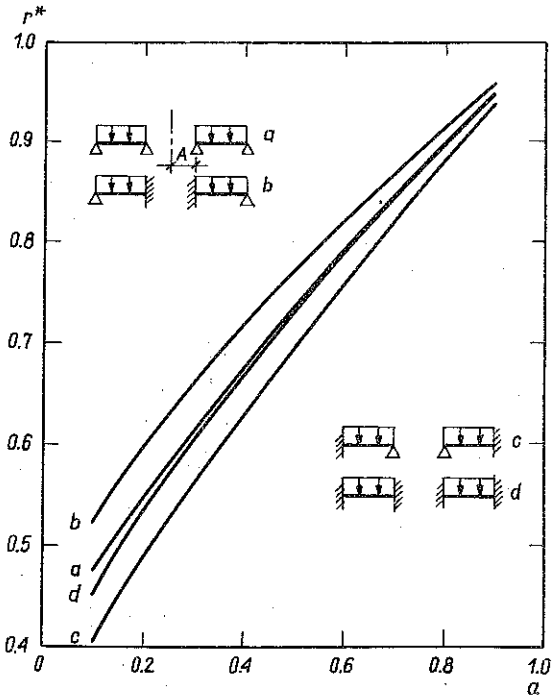


FIG. 16.

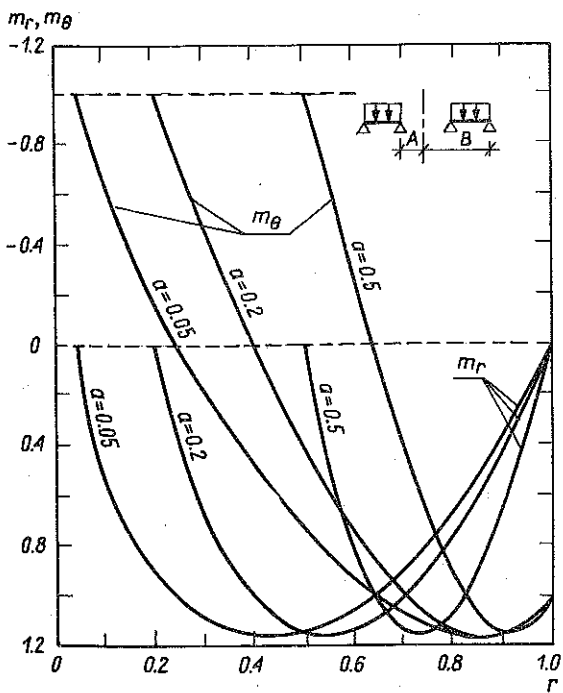


FIG. 17.

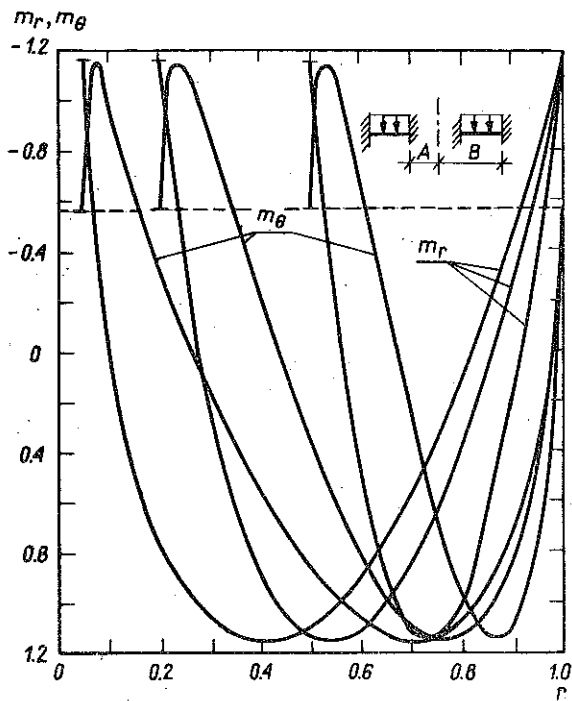


FIG. 18.

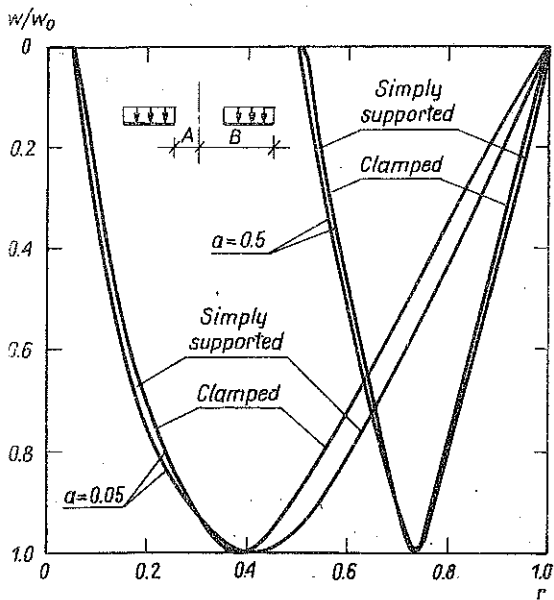


FIG. 19.

7. STATICALLY INDETERMINATE PLATES

Annular plates supported at both boundaries and uniformly loaded on the entire surface have the load carrying capacities as given in Table 7. The stress profile for such structures at collapse runs over a large part of the yield curve (3.1) and involves both Eq. (3.12) and (3.16). The stress regime change takes place at $r=r^*$ following from Eq. (3.11) and corresponds to the stress point B in Fig. 2. Positions of the transition radius are given in Fig. 16. The value of the reaction at the internal circumference follows from the solution of the coupled moment-deflection velocity system of equations as explained in Section 3. A dimensionless parameter β specifying the reaction is given in Table 7. Partial results regarding this type of plates were given by OSCHATZ [11].

Figs. 17 and 18 illustrate the bending moment fields in the considered plates for two cases of boundary conditions. Further examples can be found in [15]. For the sake of completeness, deflection velocities are plotted in Fig. 19, indicating the stress profile transition radius r^* .

8. CONCLUDING REMARKS

The tables and diagrams presented in this paper constitute a comprehensive collection of design data for plates obeying the Huber-Mises yield condition. The results were obtained at the issue of a systematic study and checked with the partial results already available in the literature. The tables are original and all the diagrams result from the computations performed with the program described in [15, 16] and allow to study also statically indeterminate annular plates.

ACKNOWLEDGEMENT

The results presented in this paper were obtained in the course of studies within the Task 02.1 Engineering Plasticity of the Research Project 05.12 sponsored by the Polish Academy of Sciences.

REFERENCES

1. W. PRAGER, *An introduction to plasticity*, Addison-Wesley, Reading, Mass., 1959.
2. P. G. HODGE, Jr., *Plastic analysis of structures*, McGraw Hill, New York 1959.
3. A. SAWCZUK, Th. JAEGER, *Grenztragfähigkeits-Theorie der Platten*, Springer, Berlin 1963.
4. P. G. HODGE, Jr., *Plastic analysis of rotationally symmetric plates and shells*, Prentice Hall, Englewood Cliffs, N.J., 1963.
5. D. NIEPOSTYN, *Nośność graniczna płyt kołowo-symetrycznych*, Biblioteka Inżynierii i Budownictwa, 3, Arkady, Warszawa 1963.

6. S. KALISZKY, *Vasbeton lemezek méretezése a képlékenységtan szerint*, Müszaki Könyvkiadó, Budapest 1967.
7. M. A. SAVE, C. E. MASSONNET, *Plastic analysis and design of plates, shells and disks*, North-Holland, Amsterdam 1972.
8. A. SAWCZUK, *Plastic plates*, CISM Lecture Notes, Udine 1974.
9. H. G. HOPKINS, A. J. WANG, *Load-carrying capacities for circular plates of perfectly-plastic material with arbitrary yield condition*, J. Mech. Phys. Solids, **3**, 117-129, 1954.
10. G. EASON, *Velocity fields for circular plates with the von Mises yield condition*, J. Mech. Phys. Solids, **6**, 231-235, 1958.
11. A. OSCHATZ, *Bestimmung der Traglast von Kreis- und Kreisringplatten mit Berücksichtigung der Querkraftschubspannungen*, Z. ang. Math. Mech., **48**, 325-332, 1968.
12. H. GÜNTHER, G. BRAUNING, *Die Traglast rotationssymmetrisch belasteter Kreisplatten mit radial veränderlicher Plattendicke und Fließspannung*, Wiss. Z. d. Techn. Hochsch. Karl-Marx-Stadt, **10**, 579-581, 1968.
13. H. GÜNTHER, G. BRAUNING, *Zur Traglast anisotroper Kreisplatten*, Wiss. Z. d. Tech. Hochsch. Karl-Marx-Stadt, **14**, 587-592, 1972.
14. G. GUERLEMENT, D. O. LAMBLIN, *Analyse limite de plaques circulaires avec la condition de plasticité de von Mises*, Bull. Tech. Suisse Romande, **98**, 1-8, 1972.
15. J. SOKÓL-SUPEL, A. GRABARSKI, A. SAWCZUK, *Nośność graniczna metalowych płyt kołowych*, Prace IPPT, **41/1975**, Warszawa 1975.
16. J. SOKÓL-SUPEL, *Numeryczna metoda wyznaczania nośności granicznej płyt kołowo-symetrycznych*, Rozpr. Inż., **26**, **1**, 179-191, 1978.
17. R. J. ROARK, *Formulas for stress and strain*, McGraw-Hill, New York 1965.
18. V. V. SOKOLOVSKI, *Elastic-plastic bending of circular and annular plates* (in Russian), Prikl. Math. Mekh., **8**, 141-166, 1944.
19. V. V. SOKOLOVSKI, *Theory of plasticity* (in Russian), Nauka, Moscow 1969.
20. Y. OHASHI, S. MURAKAMI, *Study on the axisymmetric elasto-plastic deformation of thin plates*, Mem. Fac. Engng. Nagoya Univ., **20**, 355-433, 1968.
21. Y. OHASHI, S. MURAKAMI, *Axisymmetric elasto-plastic deformation of circular plates under combined action of lateral load and membrane force*, Mem. Fac. Engng. Nagoya Univ., **21**, 79-121, 1969.
22. R. M. HAYTHORTHWAITE, *The deflection of plates in the elastic-plastic range*, Proc. 2nd US Nat. Congr. Appl. Mech. (Ann Arbor, 1954), ASME 521-526, New York 1955.
23. A. A. ILIUSHIN, *Plasticity* (in Russian) Gostiechizdat, Moscow 1948.

STRESZCZENIE

NOŚNOŚĆ GRANICZNA OBROTOWO-SYMETRYCZNYCH PŁYT DLA WARUNKU HUBERA-MISESA

Przedmiotem pracy jest obrotowo-symetryczne zginanie sztywno-plastycznych płyt. Materiał płyty uplastycznia się zgodnie z warunkiem plastyczności Hubera-Misesa. Zaproponowano procedurę numeryczną do obliczania nośności granicznej dowolnie obciążonych, okrągłych i pierścieniowych płyt, także statycznie niewyznaczalnych. Praca uzupełniona jest zestawem tablic i wykresów, które podają dane do projektowania płyt metalowych dla praktycznie ważnych przypadków obciążeń.

Резюме

ПРЕДЕЛЬНАЯ НЕСУЩАЯ СПОСОБНОСТЬ ВРАЩАТЕЛЬНО-СИММЕТРИЧНЫХ ПЛИТ ДЛЯ УСЛОВИЯ ГУБЕРА-МИЗЕСА

Предметом работы является вращательно-симметричный изгиб жестко-пластических плит. Материал плиты переходит в пластическое состояние согласно условию пластичности Губера-Мизеса. Предложена численная процедура для расчета предельной несущей способности произвольно нагруженных, круглых и кольцевых плит, также статически неопределенных. Работа дополнена комплектом таблиц и графиков, которые приводят данные для проектирования металлических плит для практически важных случаев нагрузок.

POLISH ACADEMY OF SCIENCES
INSTITUTE OF FUNDAMENTAL TECHNOLOGICAL RESEARCH

Received September 8, 1977.
